Biochimica et Biophysica Acta 1837 (2014) 159–166

Contents lists available at ScienceDirect

Biochimica et Biophysica Acta

journal homepage: www.elsevier.com/locate/bbabio

Influence of the Ca^{2+} ion on the Mn_4Ca conformation and the H-bond network arrangement in Photosystem II

Keisuke Saito, Hiroshi Ishikita *

Department of Biological Sciences, Graduate School of Science, Osaka University, Machikaneyama-cho 1–1, Toyonaka 560-0043, Japan
Japan Science and Technology Agency (JST), PRESTO, 4-1-8 Honcho Kawaguchi, Saitama 332–0012, Japan

ARTICLE INFO

Article history:
Received 2 April 2013
Received in revised form 19 September 2013
Accepted 24 September 2013
Available online 2 October 2013

Keywords:
Ca-depleted Photosystem II
Mn_4Ca
Distorted Mn_3CaO_4 cubane
Sr-substituted photosystem II
Overreduced state

ABSTRACT

In the crystal structure of Photosystem II (PSII) analyzed at a resolution of 1.9 Å, most of the bond lengths between Mn and O atoms in the oxygen-evolving Mn_4Ca cluster are 1.8–2.1 Å. On the other hand, the Mn1 – O5 bond in the Mn_3CaO_4 cubane region of the Mn_4Ca cluster is significantly elongated to 2.6 Å. Using a quantum mechanical/molecular mechanical approach, we investigated factors that are responsible for distortion of the Mn_3CaO_4 cubane. Removal of Ca led to shortening the Mn1 – O5 bond by 0.2 Å; however, Mn1 – O5 remained significantly elongated, at >2.5 Å. Conversely, removal of Mn4 significantly shortens the Mn1 – O5 distance by 0.5 Å to 2.2 Å, resulting in a more symmetric cubane shape. These results suggest that Mn4, not Ca, is predominantly responsible for distortion of the Mn_3CaO_4 cubane. It was not the Ca component that was responsible for the existence of the two S2 conformers but two different Mn oxidation states (Mn1, Mn2, Mn3, M4) = (III, IV, IV, IV) and (IV, IV, IV, III); they were interconvertible by translocation of the O5 atom along the Mn1–O5–Mn4 axis. Depletion of Ca resulted in rearrangement of the H-bond network near TyrZ, which proceeds via a chloride ion (Cl-1 pathway). This may explain why Ca depletion inhibits the S2 to S3 transition, the same process that can also be inhibited by Cl^- depletion.

1. Introduction

The heart of the Photosystem II (PSII) reaction center consists of the D1 and D2 subunits, which form a quasi-symmetrical complex that contains cofactors arranged to span the transmembrane protein in 2 branches. From the lumenal to the stromal side of the complex, the following cofactors are present: an overlapping pair of chlorophyll *a* (Chl*a*) molecules (P_{D1}/P_{D2}), 2 monomeric Chl*a* molecules (Chl_{D1}/Chl_{D2}), 2 pheophytins, and 2 quinone molecules (see Ref. [1] for the most recent crystal structure). Excitation of Chl*a* leads to charge separation on the D1 branch and formation of the cationic $[P_{D1}/P_{D2}]^{\bullet+}$ state (reviewed in Refs. [2,3]). The resulting $[P_{D1}/P_{D2}]^{\bullet+}$ state serves as an electron abstractor for the oxygen-evolving Mn_4Ca cluster via the redox-active tyrosine D1-Tyr161.

The PSII crystal structure from *Thermosynechococcus vulcanus* has been recently reported at a resolution of 1.9 Å, which exposes all of the components of the oxygen-evolving Mn_4Ca cluster, and identifies a chemical formula of Mn_4CaO_5 [1] (Fig. 1). The overall shape of the Mn_4Ca cluster resembles a "distorted chair" form (Figs. 1 and 2), which consists of the Mn_3CaO_4 cubane region (Mn1, Mn2, Mn3, Ca, O1, O2, O3, and O5) and the external, back of the chair region (Mn4 and O4). Although O1, O2, and O3 are likely to be unprotonated O^{2-}, based on observations of the Mn_4Ca cluster geometry, the protonation states of O4 linking Mn4 and Mn3 in the Mn_3CaO_4-cubane, and O5 in one of the corners of the cubane linking Mn4 and the cubane, require further investigation. In particular, O5 might be O^{2-}, protonated OH^- [1,4,5], or H_2O [6]. Notably, recent spectroscopic studies suggested that O5 could be one of the sites for substrate water molecules [7]. One of the puzzling characteristics of O5 is that it appears to exchange very quickly with bulk solvent water, a feature not yet observed in synthetic Mn complexes [8–10]. This fast exchange has been attributed to a number of structural factors including its ligation to the solvated Ca^{2+} ion [7]. Several studies have suggested that the O5 position is not unique between Mn1 and Mn4 but instead two discrete binding motifs [11,12], which appear to be associated with distortion of the Mn_3CaO_4 cubane region induced by the Jahn–Teller effect [13].

Most of the Mn – O bonds are in the range of 1.8–2.1 Å in the Mn_4Ca cluster, whereas the Ca–O distances are longer, in the range of 2.3–2.5 Å. The current literature consensus appears that the X-ray crystal structure does not represent the catalyst in one of its functional S-states, owing to photoreduction of the Mn_4Ca cluster via the X-ray beam (e.g., [14]). This results in the elongation of Mn–Mn distances, as compared to EXAFS data and as a consequence, all Mn–O distances (e.g., [15,16]). Indeed, DFT models based on the crystal structure typically have shorter Mn – O bonds, consistent with that observed for

Abbreviations: PSII, Photosystem II; QM/MM, quantum mechanics/molecular mechanics

* Corresponding author at: Department of Biological Sciences, Graduate School of Science, Osaka University, Machikaneyama-cho 1–1, Toyonaka 560-0043, Japan. Tel.: +81 6 6850 5422; fax: +81 6 6850 5423.
E-mail address: hiro@bio.sci.osaka-u.ac.jp (H. Ishikita).

0005-2728/$ – see front matter © 2013 Elsevier B.V. All rights reserved.
http://dx.doi.org/10.1016/j.bbabio.2013.09.013

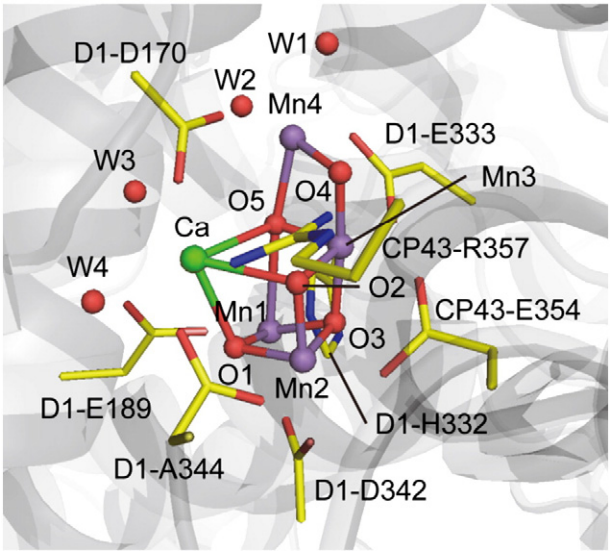

Fig. 1. Overview of the Mn_4Ca cluster in the 1.9-Å crystal structure [1].

Mn(III)/Mn(IV) model complexes (e.g., all Mn–O distances are shorter than 2.1 Å [17]).

Remarkably, two Mn – O bonds, namely Mn1 – O5 (2.6 Å) and Mn3 – O5 (2.4 Å) in the Mn_3CaO_4 cubane region, are elongated to an extent comparable to the Ca – O bonds, thereby causing distortion of the Mn_3CaO_4 cubane region [18]. Kawakami et al. have discussed the possible importance of distortion of the cubane in the process of water oxidation and O – O bond formation [18]. Indeed, synthesized inorganic Mn clusters with a shape of regular cubane are considered significantly less active in catalyzing water oxidation [19,20]. Robinson et al. reported that among synthesized inorganic Mn clusters, catalytic activity was exclusively found in distorted cubic phases of the Mn oxide polymorphs, all possessing elongated Mn – O bonds [17]. The distorted form of the cubane region therefore appears to be associated with catalytic activity

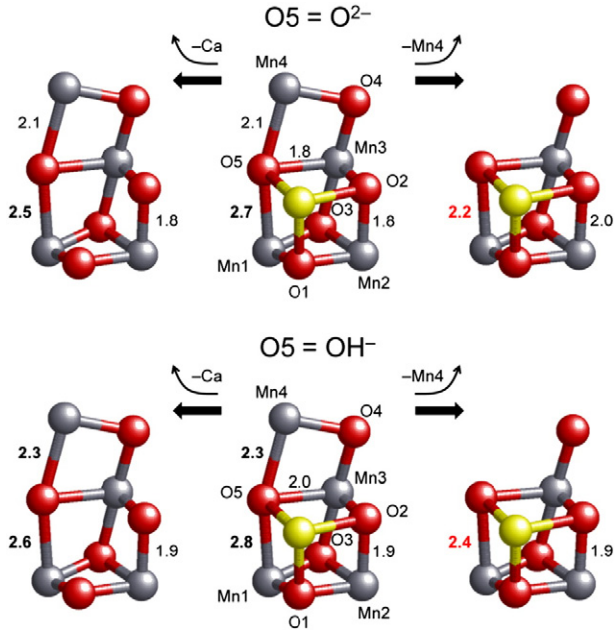

Fig. 2. Changes in Mn–O distances (Å) in the Mn_4Ca cluster (gray, yellow, and red for Mn, Ca, and O atoms, respectively) upon Ca/Mn4 depletion in the presence of O^{2-} (top) or OH^- (bottom) at O5. In each case (Mn1, Mn2, Mn3, M4) = (III, IV, IV, III) in the S1 state. Note that for clarity, not all of the atoms in the QM region are shown, but all of the ligand atoms (side chains and water molecules) are included in the QM region.

in water oxidation; as a result, factors that induce distortion of the Mn_3CaO_4 cubane region in the 1.9-Å crystal structure appear to be important in identifying the origin of the water-splitting capability in PSII.

The presence of two water molecules to the Ca implies that Ca plays an important role in the water splitting reaction. However, its function remains yet unclarified (reviewed in Ref. [21]). Kawakami et al. have noted that the inclusion of Ca in the Mn_4Ca cluster results in a distorted cubane structure [18]. Notably, the two elongated Mn – O bonds, Mn1 – O5 and Mn3 – O5, are shared by O5, which is linked with the Ca component (Ca–O5 = 2.5 Å) [1]. If the Ca component significantly contributes to inducing distortion of the cubane, the distorted cubane would be relaxed to form a more symmetric cubane upon Ca depletion. On the other hand, the (electronic) structure of the Mn_4Ca cluster remains essentially unaltered upon Ca depletion in Mn K-edge X-ray absorption spectroscopy [22] and ENDOR [23] studies. The same phenomenon has also been reported in the Sr-substituted Mn_4 cluster. Sr performs the role of Ca in O_2-evolving activity, with approximately 40% efficiency of the Mn_4Ca cluster [24–26]. The crystal structure of the Sr-substituted PSII suggests that the Sr-substituted Mn_4Sr cluster is very similar to the Mn_4Ca cluster [27], as has already been noted in EPR [24,28] and EXAFS [29] studies. (Note: in cyanobacteria, Ca cannot be removed or replaced in isolated PSII, and they must be substituted in the culture medium with Sr [30].) In addition, even upon Ca depletion, Mn atoms can be oxidized, although the cluster cannot progress S-state transitions beyond the S2 state [24,31–33]. These results imply a role of Ca in the function of the Mn_4Ca cluster beyond an integral structural component, as has been indicated by ENDOR studies [23].

In the present study, we used a large-scale quantum mechanics/molecular mechanics (QM/MM) approach to identify factors responsible for distortion of the Mn_3CaO_4 cubane in the 1.9-Å crystal structure.

2. Computational procedures

2.1. Coordinates and atomic partial charges

The atomic coordinates of PSII were taken from the X-ray structure of the PSII monomer unit designated monomer A of the PSII complexes from *T. vulcanus* at a 1.9-Å resolution (PDB code, 3ARC) [1]. Hydrogen atoms were generated and energetically optimized with CHARMM [34], whereas the positions of all non-hydrogen atoms were fixed, and all titratable groups were kept in their standard protonation states (i.e., acidic groups were ionized and basic groups were protonated). For QM/MM calculations, we used additional counter ions to neutralize the entire system. Atomic partial charges of the amino acids were adopted from the all-atom CHARMM22 [35] parameter set. The atomic charges of Chl*a*, Pheo*a*, and quinones were those reported in our previous study on PSII [36].

2.2. QM/MM calculations

We used the Qsite [37] program code as used in a previous study [38]. We employed the unrestricted DFT method with the B3LYP functional and LACVP* basis sets. The geometries were refined by constrained QM/MM optimization. Specifically, the coordinates of the heavy atoms in the surrounding MM region were fixed to the original X-ray coordinates, whereas those of the H atoms in the MM region were optimized using the OPLS2005 force field. All of the atomic coordinates in the QM region were fully relaxed (i.e., not fixed) in the QM/MM calculation. Note that the resulting atomic coordinates of the QM region essentially did not alter upon full relaxation of the entire atoms (including heavy atoms) in the surrounding MM region (Table S1).

The QM region was defined as [Mn_4CaO_5 and all of the ligand residues and ligand water molecules shown in Fig. 1] for the Mn_4Ca cluster or [Mn_4CaO_5 and all of the ligand residues, ligand water molecules, and most of the water molecules in the diamond-shaped water cluster [38]

near D1-Tyr161/D1-His190 moiety (i.e., W3, W5, and W6 [18])] for the Ca-depleted Mn_4 cluster and the Mn4–depleted Mn_3Ca cluster. Upon deletion of Mn4, O4 was modeled as OH^-. All other protein units and cofactors were approximated by the MM force field. It has been suggested that the ground state of the Mn_4Ca cluster is considered to be either a singlet or quintet in EPR studies [39–41]. On the other hand, as considered in previous theoretical studies (e.g., [42,43]), the cluster was considered to be in the S1 state with ferromagnetically coupled Mn atoms in QM/MM calculations, (Mn1, Mn2, Mn3, M4) = (III, IV, IV, III) and the total spin $S = 7$ for the intact Mn_4Ca and Ca-depleted Mn_4 clusters, whereas (Mn1, Mn2, Mn3) = (III, IV, IV) and $S = 5$ for the Mn4–depleted Mn_3Ca and Mn_4/Ca-depleted Mn_3 clusters (for the QM/MM optimized geometries, see Supporting PDB file. For calculated spin densities, see Table S2). Note that the resulting optimized Mn_4Ca geometry appears not to be crucial to the spin configurations, as demonstrated in previous theoretical studies [42,43].

The potential-energy profile of the Mn1–O5–Mn4 bond was obtained as follows: first, we prepared for the QM/MM optimized geometry without constraints, and we took the resulting geometry as the initial geometry. The O5 atom was then moved along the Mn1–Mn4 axis by 0.05 Å, after which the geometry was optimized by constraining the Mn1–O5 (or Mn4–O5) distances, and the energy of the resulting geometry was calculated. This procedure was repeated until the O5 atom reached the Mn1 or Mn4 moiety. See text in SI for evaluation of the resulting Mn_4Ca geometries.

3. Results and discussion

In the 1.9-Å crystal structure [1], the Mn1–O5 (2.6 Å) and Mn4–O5 (2.5 Å) bonds were significantly elongated relative to the other Mn–O bonds (1.9 to 2.1 Å). In the QM/MM geometry, the two bonds were also significantly elongated (2.8 Å and 2.3 Å, respectively, in the presence of OH^- at O5) relative to other Mn–O bonds (1.8 to 2.0 Å) in the intact PSII (Fig. 2, Tables 1 and 2). O5 was migrated more toward Mn4 than Mn1 in the QM/MM geometry; the same tendency has also been observed in other theoretical studies [42,44]. Although the Mn3 – O5 bond was significantly elongated to 2.4 Å in the 1.9-Å crystal structure [1], the QM/MM geometry resulted in a shorter bond distance of 1.8–2.0 Å in the S1, i.e., (Mn1, Mn2, Mn3, Mn4) = (III, IV, IV, III) in the present study (Table 2). This indicates that the Mn_4Ca cluster in the 1.9-Å crystal structure is in a S-state lower than S1 [5,14,45], possibly with Mn3(III), that contributes to lengthening the Mn3 – O5 due to the Jahn–Teller effect.

Because the main purpose of this study is to identify factors responsible for distortion of the Mn_3CaO_4 cubane in the 1.9-Å crystal structure, these computational results, which have also been reported in previous theoretical studies [4–6,11,42,43,45], are sufficiently accurate for our purpose to describe the chemical properties of the Mn_4Ca cluster.

Table 1
Experimental (PDB: 3ARC [1]) and calculated Mn–Mn distances (in angstrom) for the intact Mn_4Ca cluster (intact) in the presence of O^{2-} or OH^- at O5.

	3ARC	This work			
O5		O^{2-}	O^{2-}	OH^-	OH^-
Mn1, 2, 3, 4		III, IV, IV, III	III, IV, IV, III	III, IV, IV, III	III, IV, IV, III
W2		OH^-	H_2O	OH^-	H_2O
		Intact	Intact	Intact	Intact
Mn1–Mn2	2.80	2.75	2.77	2.75	2.77
Mn2–Mn3	2.90	2.77	2.75	2.76	2.74
Mn1–Mn3	3.30	3.17	3.19	3.26	3.32
Mn3–Mn4	2.94	2.71	2.73	2.88	2.90
Mn1–Mn4	4.98	4.61	4.78	4.95	5.06

Table 2
Experimental (PDB: 3ARC [1]) and calculated distances (in angstrom) for the intact Mn_4Ca cluster (intact), the Ca-depleted Mn_4 cluster (Ca depl.) and the Mn4-depleted Mn_3Ca cluster (Mn4 depl.). Significantly elongated Mn–O lengths are indicated in bold. n.d.: not determined.

O5		O^{2-}			OH^-		
Mn1, 2, 3, 4		III, IV, IV, III			III, IV, IV, III		
W2		H_2O			H_2O		
	3ARC	Intact	Ca depl.	Mn4 depl.	Intact	Ca depl.	Mn4 depl.
O1–Mn1	1.87	1.84	1.80	1.85	1.83	1.82	1.85
O1–Mn2	2.06	1.83	1.78	1.82	1.81	1.78	1.82
O1–Ca	2.33	2.36	n.d.	2.49	2.35	n.d.	2.45
O2–Mn2	2.13	1.82	1.76	1.80	1.86	1.86	1.80
O2–Mn3	1.87	1.86	1.83	1.94	1.80	1.79	1.89
O2–Ca	2.49	2.45	n.d.	2.38	2.52	n.d.	2.42
O3–Mn1	1.81	1.90	1.89	1.88	1.94	1.92	1.89
O3–Mn2	2.10	1.83	1.85	1.81	1.85	1.85	1.82
O3–Mn3	2.13	1.90	1.90	1.96	1.88	1.89	1.93
O4–Mn3	2.09	1.82	1.82	1.79	1.84	1.82	1.77
O4–Mn4	2.11	1.76	1.77	n.d.	1.78	1.79	n.d.
O5–Mn1	**2.60**	**2.72**	**2.52**	2.21	**2.84**	**2.58**	**2.38**
O5–Mn3	**2.38**	1.79	1.77	1.71	1.99	1.94	1.87
O5–Mn4	**2.50**	2.08	2.06	n.d.	**2.25**	**2.25**	n.d.
O5–Ca	2.49	2.49	n.d.	2.49	2.51	n.d.	2.49

3.1. Contribution of Ca to the stability of the Mn_4Ca cluster

In QM/MM calculations, Ca depletion did not induce a significant structural change (Fig. 3). It has been suggested that removal of factors crucial for maintaining the Mn_4Ca geometry (e.g., CP43-Arg357 and D1-His337) results in collapsing the Mn_4Ca structure [18]. Obviously, this is unlikely to be the case for the Ca component, based on observation in the QM/MM geometry of the Ca-depleted Mn_4 cluster.

Upon Ca depletion, the Mn1 – O5 bond was shortened by 0.2 Å (Fig. 2, Table 2), which appears to be sufficient to energetically compensate for the removal of Ca from the Mn_4Ca cluster. This is in line with observations in the EXAFS [22] and ENDOR [23] studies, where Ca-depletion did not result in a significant structural change in the Mn_4Ca cluster. Notably, the Mn1 – O5 bond is still remarkably long (2.5 Å), even in the Ca-depleted Mn_4 cluster (Fig. 2, Table 2). Ca binding

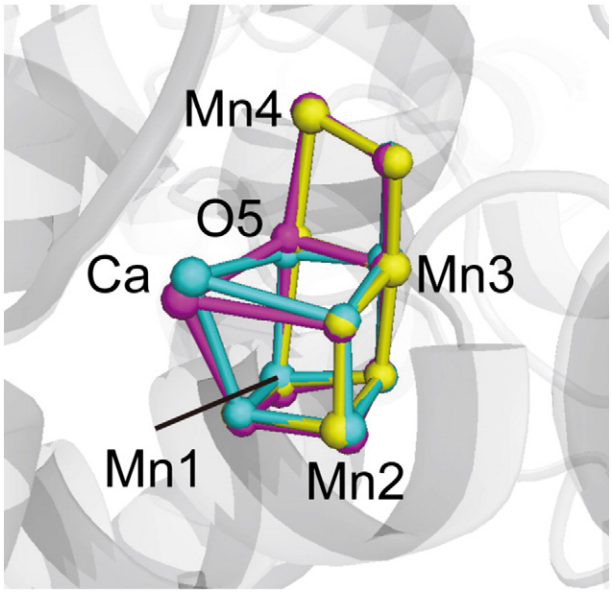

Fig. 3. Superimposition of the Mn_4Ca (pink), Ca-depleted Mn_4 (yellow) and Mn4-depleted Mn_3Ca (cyan) clusters.

at the Mn_4 cluster can therefore contribute to specifically lengthen the Mn1 – O5 bond by 0.2 Å, but is not the predominant factor for distortion of the Mn_3CaO_4 cubane observed in the 1.9-Å crystal structure.

3.2. Protonation state of O5

It has been proposed that O5 might be O^{2-}, protonated OH^- [1,4,5], or H_2O [6]. Umena et al. have proposed that O5 exists as OH^- in the S1 state [1]. Theoretical studies by Galstyan et al. [5] or Yamaguchi et al. [4] have also suggested that O5 may be OH^- in the S1 state. Recent theoretical studies by Gatt et al. [6] have suggested that O5 is a neutral water H_2O. One of the puzzling characteristics of O5 is that it appears to exchange very quickly with bulk solvent water, a feature not yet observed in synthetic Mn complexes [8–10]. ESEEM and ENDOR studies have suggested that all of the μ-oxo bridges of the Mn_4Ca cluster are deprotonated in the S2 state, and that either W1 or W2 on Mn4 is OH^- [7,46,47]. Because proton release is not observed in the S1 to S2 transition [48], it is likely that all of the μ-oxo bridges of the Mn_4Ca cluster are already deprotonated in S1.

In QM/MM calculations, protonation of O5 specifically increased the Mn3 – O5 and Mn4 – O5 bonds by 0.2 Å only when Ca exists at the binding site of the Mn_4Ca cluster (Fig. 2, Table 2). The Mn_4Ca cluster with unprotonated O5 (i.e., O5 = O^{2-}) has the Mn4 – O5 bond of 2.1 Å in the intact PSII, which is as short as the other Mn – O bond lengths, whereas the Mn_4Ca cluster with singly protonated O5 (i.e., O5 = OH^-) has a Mn4 – O5 bond of 2.3 Å. This suggests that the significantly elongated Mn4 – O5 bond in the 1.9-Å crystal structure can be best explained by the presence of OH^- at O5 than the presence of Ca. Notably, the Mn1 – O5 bond in the Mn_3CaO_4 cubane region remained almost unaffected upon protonation/deprotonation of O5. It appears therefore that the O5 protonation state is not primarily responsible for distortion of the Mn_3CaO_4 cubane.

3.3. Mn4 is primarily responsible for distortion of the cubane

Mn4 is the only Mn atom that does not belong to the Mn_3CaO_4 cubane region, located rather in the external region (Fig. 2). In particular, when O5 was unprotonated, removal of Mn4 led to a significant decrease of 0.5 Å in the Mn1 – O5 bond to 2.2 Å (Table 2). Remarkably, removal of Mn4 also affected the Mn2 – O2 bond, which was elongated to 2.0 Å (Fig. 2). In total, the difference of 0.9 Å between the Mn1 – O5 bond (2.7 Å) and the Mn2 – O2 bond (1.8 Å) in the Mn_4Ca cluster, which is the main reason for the asymmetric shape of the cubane, was significantly decreased to 0.2 Å, resulting in a more symmetric shape of the cubane (Fig. 2). These results indicate that the presence of Mn4, not Ca, is the predominant factor causing distortion of the Mn_3CaO_4 cubane of the Mn_4Ca cluster in the 1.9-Å crystal structure. Indeed, this observation can be understood by a symmetric shape of a synthetic heterometallic cubane model of the PSII Mn_4Ca cluster [49] as well as a symmetric structure of a recent Mn_3Ca cubane complex reported by Mukherjee et al. [50], which lacks a Mn atom corresponding to Mn4.

The strong interaction of O1 and O3 with Mn1 (through formation of the Mn1 – O1 and Mn1 – O3 bonds) prevents O5 from approaching Mn1 in the presence of Mn4, and O5 is therefore located away from Mn1 in the S1 state. On the other hand, Mn4 has only a single Mn – O bond (i.e., Mn4 – O4) besides the focusing Mn4 – O5 bond. This likely explains why O5 migrates more to the Mn4 moiety than the Mn1 moiety in the S1 state. The slightly lengthened Mn1 – O5 bond (2.2 Å), even in the absence of Mn4, is likely to be due to the contribution of the Jahn–Teller effect to Mn1(III). Further removal of Ca from the Mn4–depleted cluster (i.e., forming Mn_3 cluster) did not significantly affect the Mn1 – O5 length (Table S4), confirming that Mn4, rather than Ca, is the factor that increases the Mn1 – O5 length, thereby causing distortion of the Mn_3CaO_4 cubane.

3.4. Influence of Ca on the charges of the cluster

Upon Ca depletion, atomic charges of each Mn ion of the cluster essentially remained unaffected (Table 3). On the other hand, Ca depletion resulted in increase in the charges of O1, O2 and O3, and D1-Asp170 (Table 3); these O atoms are bounded to Ca in an intact cluster (Fig. 1). Because D1-Asp170 is also ligated to Mn4, D1-Asp170 was more oriented toward Mn4 upon Ca depletion (Fig. 4, left). Due to reorientation of the side chain, the induced positive charge is smaller in D1-Asp170 than in O1, O2 and O3 (Table 3). Notably, Mn4 is less positively charged in the Ca-depleted PSII (Table 3), because D1-Asp170 is exclusively ligated to Mn4 in the absence of Ca. Hence, it appears that Ca is functionally linked to Mn4 via ligation/reorientation of D1-Asp170.

3.5. Is Ca responsible for the existence of two S2 conformers?

It has been reported that the S2 state exhibits an EPR multiline signal at $g = 2.0$ (e.g., Ref. [51]) and higher signals at $g \geq 4.1$ (e.g., Ref. [52]). Recent theoretical studies by Pantazis et al. demonstrated that the two basic EPR signals originate from two energetically similar structures, conformers A and B [12]; the Mn1 – O5 bond is shorter than the Mn4 – O5 bond in conformer A, whereas the Mn4 – O5 bond is shorter than the Mn1 – O5 bond in conformer B. Remarkably, the two conformers are interconvertible by translocation of the O5 atom along the Mn1–O5–Mn4 axis [12].

We analyzed the potential energy profile of the Mn1 – O5 – Mn4 bond for the intact Mn_4Ca cluster in the PSII protein environment, by altering O5 atom position along the Mn1 – O5 or O5 – Mn4 bonds (Fig. 5). When O5 was close to Mn4 with respect to Mn1 (i.e. Mn1–O5 ≥ 2.2 Å), the Mn_4Ca cluster had (Mn1, Mn2, Mn3, Mn4) = (III, IV, IV, IV) (Fig. 5) and the geometry was similar to conformer A in Ref. [12] (Table 4). On the other hand, when O5 was close to Mn1 with respect to Mn4 (i.e. Mn1–O5 ≤ 2.2 Å), the Mn_4Ca cluster had

Table 3
Atomic partial charges (ESP charges) for the intact Mn_4Ca cluster (intact) and the Ca-depleted Mn_4 cluster (Ca depl.) in the PSII protein environment. n.d.: not determined.

O5	O^{2-}			OH^-		
	Intact	Ca depl.	Change	Intact	Ca depl.	Change
Mn1	1.40	1.45	0.06	1.34	1.33	−0.02
Mn2	1.77	1.73	−0.04	1.58	1.67	0.09
Mn3	1.90	1.91	0.00	2.00	1.93	−0.07
Mn4	1.55	1.47	−0.08	1.55	1.49	−0.06
Ca	1.74	n.d.	−1.74	1.84	n.d.	−1.84
[Mn_4Ca]	8.36	6.56	−1.80	8.31	6.41	−1.90
O1	−1.01	−0.89	0.13	−0.96	−0.85	0.11
O2	−1.15	−0.92	0.23	−1.04	−0.95	0.09
O3	−0.98	−1.00	−0.02	−0.99	−0.97	0.01
O4	−1.01	−1.05	−0.03	−1.05	−1.04	0.00
O5 [a]	−1.07	−0.90	0.17	−0.74	−0.46	0.28
[O_5]	−5.22	−4.75	0.47	−4.76	−4.27	0.49
D1-D170	−0.83	−0.77	0.06	−0.76	−0.67	0.08
D1-E189	−0.66	−0.67	−0.01	−0.61	−0.61	0.00
D1-H332	0.40	0.26	−0.14	0.42	0.35	−0.07
D1-E333	−0.47	−0.59	−0.12	−0.44	−0.48	−0.05
D1-D342	−0.62	−0.74	−0.12	−0.48	−0.64	−0.16
D1-A333	−0.64	−0.68	−0.04	−0.55	−0.60	−0.05
CP43-E354	−0.55	−0.68	−0.12	−0.37	−0.56	−0.20
CP43-R357	1.03	0.98	−0.05	1.03	1.00	−0.03
[Ligand]	−2.33	−2.88	−0.55	−1.75	−2.22	−0.46
W1	0.07	0.07	−0.01	0.09	0.08	−0.01
W2	0.12	0.01	−0.12	0.14	0.03	−0.11
W3	0.00	−0.01	−0.01	−0.01	0.00	0.01
W4	0.00	−0.05	−0.05	−0.02	−0.08	−0.06
W5	n.d.	0.01	0.01	n.d.	0.00	0.00
W6	n.d.	0.04	0.04	n.d.	0.04	0.04
[Water]	0.19	0.07	−0.12	0.20	0.08	−0.12

[a] Including charges of the bound H atoms (O5 = OH^-).

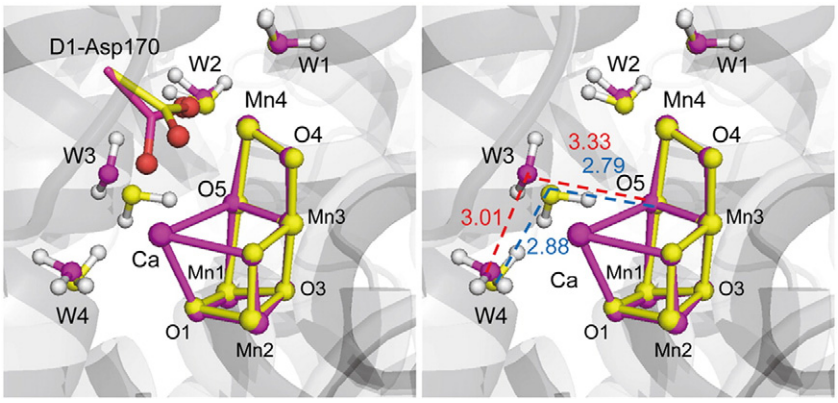

Fig. 4. Rearrangement of the ligand water molecules (W1 to W4) upon Ca depletion; intact Mn_4Ca (pink) and Ca-depleted Mn_4 (yellow) clusters. (Left) Rearrangement of the D1-Asp170 side chain. (Right) Formation of an H – bond between W3 and O5 in the Ca-depleted PSII. For clarity, the D1-Asp170 side chain is not shown.

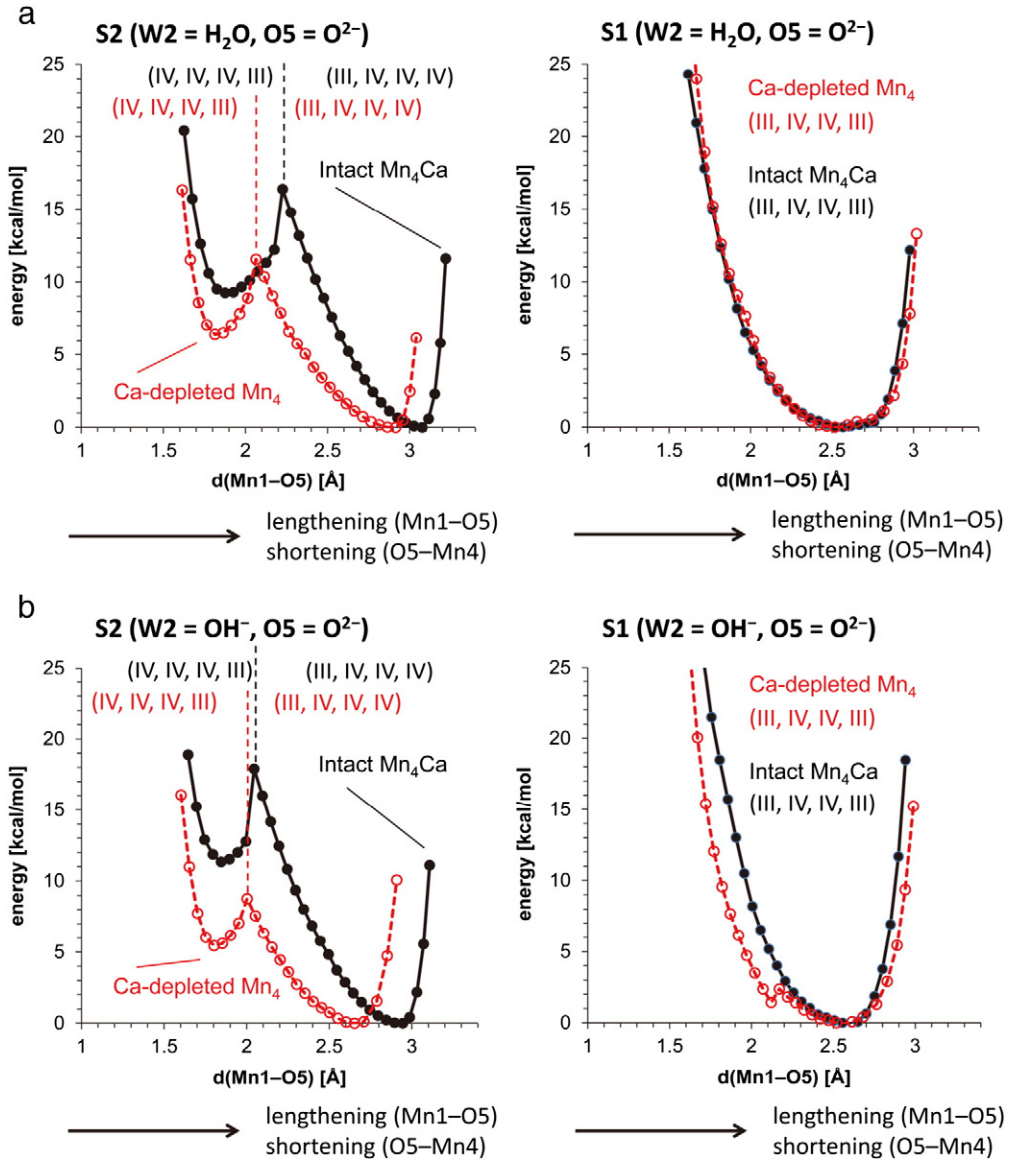

Fig. 5. Potential-energy profiles for the O5 ($=O^{2-}$) atom between Mn1 and Mn4 for the intact Mn_4Ca cluster (black solid curves) and the Ca-depleted Mn_4 cluster (red dotted curves) in the S1 (right) and S2 (left) states. (a) W2 = H_2O. (b) W2 = OH^-. The horizontal axis indicates the Mn1–O5 distance, which practically describes movement of the O5 atom between Mn1 and Mn4 moieties. Vertical dotted lines indicate the O5 positions at which the valence of (Mn1, Mn2, Mn3, M4) alters. Note that the energy minimum is set to 0 kcal/mol for each curve.

Table 4
Geometries of the two S2 conformers (in angstrom). n.d.: not determined.

	3ARC	This work		Pantazis et.al. [a]	This work		Pantazis et.al. [a]
O5		O^{2-}					
Mn1, 2, 3, 4		III, IV, IV, IV (conformer A [a])			IV, IV, IV, III (conformer B [a])		
W2		H_2O		OH^-	H_2O		OH^-
		Intact	Ca depl.	Intact	Intact	Ca depl.	Intact
O1–Mn1	1.87	1.85	1.81	1.87	1.82	1.78	1.85
O1–Mn2	2.06	1.81	1.78	1.87	1.81	1.79	1.89
O1–Ca	2.33	2.34	n.d.	2.49	2.34	n.d.	2.51
O2–Mn2	2.13	1.85	1.79	1.82	1.83	1.78	1.82
O2–Mn3	1.87	1.80	1.78	1.84	1.83	1.79	1.84
O2–Ca	2.49	2.53	n.d.	2.62	2.51	n.d.	2.59
O3–Mn1	1.81	1.94	1.90	1.93	1.85	1.84	1.89
O3–Mn2	2.10	1.86	1.87	1.92	1.84	1.86	1.92
O3–Mn3	2.13	1.86	1.88	2.01	1.88	1.90	1.97
O4–Mn3	2.09	1.85	1.83	1.81	1.82	1.82	1.80
O4–Mn4	2.11	1.75	1.76	1.90	1.76	1.78	1.87
O5–Mn1	2.60	3.08	2.91	3.21	1.90	1.85	1.87
O5–Mn3	2.38	1.91	1.87	1.85	1.89	1.87	1.90
O5–Mn4	2.50	1.79	1.78	1.87	2.92	2.62	3.16
O5–Ca	2.49	2.58	n.d.	2.72	2.58	n.d.	2.73

[a] See Ref. [12].

(Mn1, Mn2, Mn3, Mn4) = (IV, IV, IV, III) (Fig. 5) and the geometry was similar to conformer B in Ref. [12] (Table 4). The two conformers were almost isoenergetic in theoretical studies by Pantazis et al. [12], whereas the conformer A-like structure was somewhat stable with respect to the conformer B-like structure in the present study (Fig. 5); this may be due to the difference in e.g., the QM size (~240 atoms [12] and ~110 atoms), the absence/presence of the MM region as a protein environment (absent [12] and present), spin configuration (antiferromagnetic [12] and ferromagnetic), and the protonation state of D1-His337 (positively charged [12] and neutral, respectively).

To evaluate if Ca contributes to the existence of the two S2 conformers, we also analyzed the potential energy profile of the Mn1 – O5 – Mn4 bond for the Ca-depleted Mn_4 cluster. The resulting potential energy curve for the Ca-depleted Mn_4 cluster resembles that for the intact Mn_4Ca cluster, which demonstrates the existence of the two S2 conformers with (Mn1, Mn2, Mn3, Mn4) = (III, IV, IV, IV) and (IV, IV, IV, III) in the absence of Ca (Fig. 5). The two S2 conformers exist irrespective of the protonation state of W2, i.e., W2 = H_2O (Fig. 5a) or OH^- (Fig. 5b). Interestingly, the potential energy curve obtained for the S1 state possesses a single energy minimum in both the intact Mn_4Ca and Ca-depleted Mn_4 clusters; this suggests that there exists only a single conformer in the S1 state (Fig. 5).

Thus, it can be concluded that Ca is not required for generating two conformers in the S2 state. This is consistent with EPR studies; the S2 state responsible for the multiline signal (conformer A [12] or the (III, IV, IV, IV) conformer in Figs. 5 and 6) can be converted to the state responsible for the $g = 4.1$ signal (conformer B [12] or the (IV, IV, IV, III) conformer in Figs. 5 and 6) upon the absorption of infrared light in the Ca-depleted PSII [52–54]. Indeed, the Mn_4 cluster can form the S2 state even in the absence of Ca [24,31–33]. It appears that incapability of the Ca-depleted Mn_4 cluster to progress S-state transitions beyond the S2 state [24,31–33] is not due to significant changes in the electronic structure of the cluster but due to other factors, e.g., alterations in an H-bond network, which may play a key role in a proton transfer event in the S state transitions (discussed later).

The two conformers in the S2 state can be interconvertible by an electron transfer from an electron donor Mn(III) to an electron acceptor Mn(IV), which is induced by approach of O5 to an electron donor Mn(III) (Fig. 6). Such an electron transfer event is possible only in the specific oxidation state $Mn(IV)_3Mn(III)$ (i.e., S2), where Mn(IV) must be reduced concertedly to oxidize Mn(III) in the Mn_4Ca cluster; this is

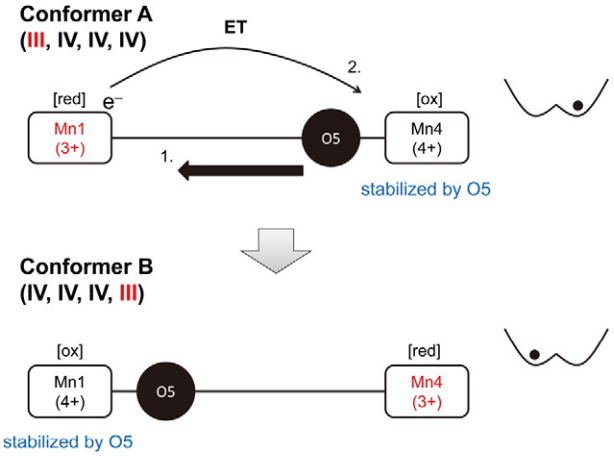

Fig. 6. Interconversion of the two conformers in the S2 state in response to movement of the O5 atom and electron transfer between Mn(III) and Mn(IV). [red] and [ox] indicate reduced and oxidized states (i.e., Mn(III) and Mn(IV)), respectively.

supported by the absence of the corresponding interconvertible conformers in the S1 state (Fig. 5).

3.6. Possible mechanism of inhibition of the S state transition: Ca depletion and Cl^- depletion

We observed that Ca depletion induced reorientation/displacement of water molecules near the Mn_4Ca cluster, including the ligand water molecules of Ca, W3 and W4 (Fig. 4). Among the water molecules, W3 underwent a significant displacement upon Ca depletion, whereas W4 almost remained at the original position in the crystal structure (Fig. 4). The same tendency has also been reported in the Sr-substituted Mn_4 cluster, where upon substitution of Ca with Sr, the Sr – O bond is predominantly elongated for W3, not for W4 [27]. The larger mobility of W3 relative to W4 may be due to the fact that W3 has only water molecules as an H-bond partner, whereas W4 has side chains of D1-Tyr161 (TyrZ) and D1-Gln165. Hence, it appears that the W3 position is more significantly linked with the presence of Ca (or e.g., Sr) than the W4 position.

O5 has no H-bond partner in the 1.9-Å crystal structure [1]. On the other hand, Ca depletion leads to formation of an H-bond between O5 and W3 (O_{W3}–O5 = 2.79 Å, Fig. 4). In addition, displacement of the W3 position upon Ca depletion also leads to significant rearrangement of the H-bond network near TyrZ (Fig. 7). In particular, "the diamond-shaped cluster (W3 and W5—W7)", which has been reported to play a role in forming the unusually short H – bond (≤2.5 Å [1]) between TyrZ and D1-His190 [38], disappears in the corresponding H-bond network in the Ca-depleted PSII (Fig. 7).

Remarkably, this region is also a part of an H-bond network that proceeds toward the protein bulk surface via a chloride ion, Cl-1 (the Cl-1 pathway) (Fig. 8) [55]. Because Cl^- is required to progress through the S2 to S3 [56,57] and S3 to S0 transitions [58], it has been proposed that the Cl-1 pathway may be active specifically for the S2 to S3 or S3 to S0 transitions [55]. Thus, the H-bond network of the Cl-1 pathway can also be affected by Ca depletion. This may explain why the S2 to S3 transition is commonly inhibited in both the Ca-depleted [24,31–33] and Cl^--depleted [56,57] PSII.

4. Concluding remarks

Using a QM/MM approach and the 1.9-Å crystal structure, we were able to clarify factors that affect distortion of the Mn_3CaO_4 cubane region of the Mn_4Ca cluster in the PSII protein environment. The geometry of the Mn_4Ca remained essentially unaltered upon Ca depletion (Fig. 3), as already suggested in Mn K-edge X-ray absorption spectroscopy [22]

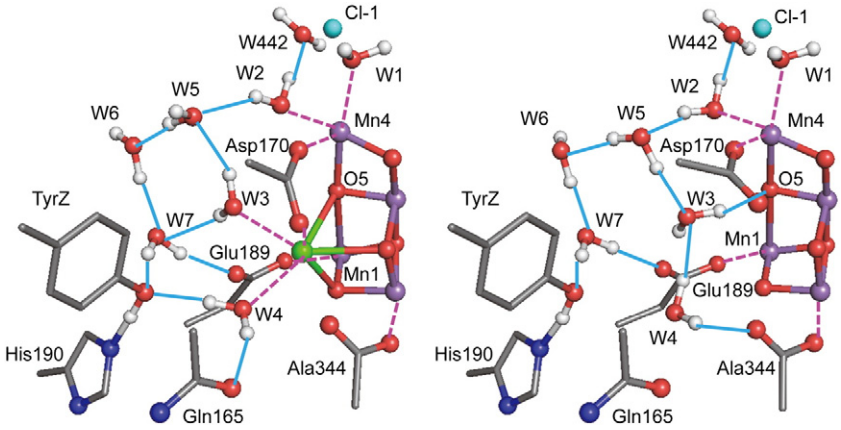

Fig. 7. H – bond (blue solid line) patterns in the intact PSII (left) and Ca-depleted PSII (right). Red dotted lines indicate ligation to the Mn_4Ca cluster. TyrZ, D1-Gln165, D1-His190, and W7 are included in the MM region, whereas all of the other groups are included in the QM region.

and ENDOR [23] studies. The Ca component at the binding site contributes to lengthening the Mn1 – O5 bond by 0.2 Å. However, the Mn1 – O5 length was 2.5 Å, which was significantly long even in the absence of Ca (Fig. 2), indicating that the Ca component is not primarily responsible for distortion of the Mn_3CaO_4 cubane region. On the other hand, removal of Mn4 significantly shortened the Mn1 – O5 bond to 2.2 Å, significantly eliminating distortion of the Mn_3CaO_4 cubane (Fig. 2). Therefore, the presence of Mn4, and not Ca, is the predominant factor that causes distortion of the Mn_3CaO_4 cubane in the 1.9-Å crystal structure. Mn4, which is located in the external region of the cubane, plays a role in weakening the Mn1 – O5 bond and possibly increasing or tuning the reactivity of O5 during the water oxidation reaction.

Two interconvertible S2 conformers [12] were observed irrespective of the presence/absence of the Ca component. The potential energy curve for the Ca-depleted Mn_4 cluster resembles that for the intact Mn_4Ca cluster (Fig. 5). Thus, Ca is not directly responsible for the flexible coordination of O5 along the Mn1–Mn4 axis. Instead, we clarified that the two conformers have different valence of (Mn1, Mn2, Mn3, Mn4) = (III, IV, IV, IV) and (IV, IV, IV, III), which is interconvertible only in the S2 state via electron transfer between Mn1 and Mn4 (Fig. 6). The corresponding two interconvertible conformers are absent in the S1 state (Fig. 5).

Ca depletion induces rearrangement of an H-bond network near TyrZ (including the diamond-shaped water cluster [38], Fig. 7), which also proceeds via Cl-1 toward the protein bulk surface (Cl-1 pathway [55], Fig. 8). Rearrangement of the H-bond network of the Cl-1 pathway upon Ca depletion may explain why both Ca-depletion [24,31–33] and Cl^--depletion [56,57] commonly inhibit the S2 to S3 transition. These results provide insights that help our understanding of the assembly of the Mn_4Ca cluster as well as the reaction mechanism of water oxidation.

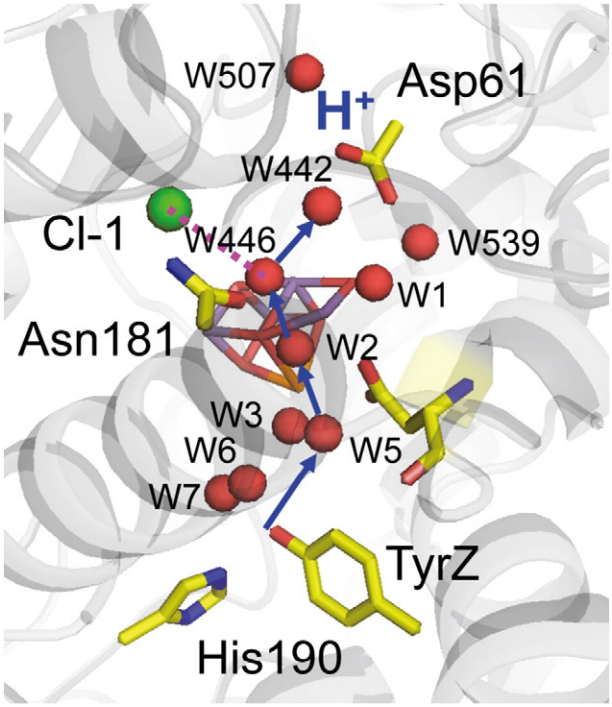

Fig. 8. An H – bond network (the Cl-1 pathway) that proceeds from the TyrZ moiety via a chloride ion, Cl-1 [55].

Acknowledgement

This research was supported by the JST PRESTO program (K.S.), Grant-in-Aid for Scientific Research from the Ministry of Education, Culture, Sports, Science and Technology (MEXT) of Japan (22740276 to K.S. and 25107517 to H.I.), and Takeda Science Foundation (H.I.).

Appendix A. Supplementary data

Supplementary data to this article can be found online at http://dx.doi.org/10.1016/j.bbabio.2013.09.013.

References

[1] Y. Umena, K. Kawakami, J.-R. Shen, N. Kamiya, Crystal structure of oxygen-evolving photosystem II at a resolution of 1.9 Å, Nature 473 (2011) 55–60.
[2] B.A. Diner, F. Rappaport, Structure dynamics, and energetics of the primary photochemistry of photosystem II of oxygenic photosynthesis, Annu. Rev. Plant Biol. 53 (2002) 551–580.
[3] G. Renger, T. Renger, Photosystem II: the machinery of photosynthetic water splitting, Photosynth. Res. 98 (2008) 53–80.
[4] K. Yamaguchi, H. Isobe, S. Yamanaka, T. Saito, K. Kanda, M. Shoji, Y. Umena, K. Kawakami, J.-R. Shen, N. Kamiya, M. Okumura, Full geometry optimizations of the mixed-valence $CaMn_4O_4X(H_2O)_4$ (X = OH or O) cluster in OEC of PS II: degree of symmetry breaking of the labile Mn–X–Mn bond revealed by several hybrid DFT calculations, Int. J. Quantum Chem. (2012), http://dx.doi.org/10.1002/qua.24117.
[5] A. Galstyan, A. Robertazzi, E.W. Knapp, Oxygen-evolving Mn cluster in photosystem II: the protonation pattern and oxidation state in the high-resolution crystal structure, J. Am. Chem. Soc. 134 (2012) 7442–7449.
[6] P. Gatt, S. Petrie, R. Stranger, R.J. Pace, Rationalizing the 1.9 Å crystal structure of photosystem II—a remarkable Jahn–Teller balancing act induced by a single proton transfer, Angew. Chem. Int. Ed. Engl. 51 (2012) 12025–12028.
[7] L. Rapatskiy, N. Cox, A. Savitsky, W.M. Ames, J. Sander, M.M. Nowaczyk, M. Rogner, A. Boussac, F. Neese, J. Messinger, W. Lubitz, Detection of the water-binding sites of the oxygen-evolving complex of Photosystem II using W-band ^{17}O electron–electron double resonance-detected NMR spectroscopy, J. Am. Chem. Soc. 134 (2012) 16619–16634.

[8] R. Tagore, H. Chen, R.H. Crabtree, G.W. Brudvig, Determination of mu–oxo exchange rates in di–mu–oxo dimanganese complexes by electrospray ionization mass spectrometry, J. Am. Chem. Soc. 128 (2006) 9457–9465.
[9] R. Tagore, R.H. Crabtree, G.W. Brudvig, Distinct mechanisms of bridging-Oxo exchange in Di–μ–O dimanganese complexes with and without water-binding sites: implications for water binding in the O_2-evolving complex of Photosystem II, Inorg. Chem. 46 (2007) 2193–2203.
[10] I.L. McConnell, V.M. Grigoryants, C.P. Scholes, W.K. Myers, P.Y. Chen, J.W. Whittaker, G.W. Brudvig, EPR-ENDOR characterization of (^{17}O, ^{1}H, ^{2}H) water in manganese catalase and its relevance to the oxygen-evolving complex of photosystem II, J. Am. Chem. Soc. 134 (2012) 1504–1512.
[11] M. Kusunoki, S1-state Mn_4Ca complex of Photosystem II exists in equilibrium between the two most-stable isomeric substates: XRD and EXAFS evidence, J. Photochem. Photobiol. B 104 (2011) 100–110.
[12] D.A. Pantazis, W. Ames, N. Cox, W. Lubitz, F. Neese, Two interconvertible structures that explain the spectroscopic properties of the oxygen-evolving complex of Photosystem II in the S2 state, Angew. Chem. Int. Ed. Engl. 51 (2012) 9935–9940.
[13] K. Yamaguchi, S. Yamanaka, H. Isobe, T. Saito, K. Kanda, Y. Umena, K. Kawakami, J.-R. Shen, N. Kamiya, M. Okumura, H. Nakamura, M. Shoji, Y. Yoshioka, The nature of chemical bonds of the $CaMn_4O_5$ cluster in oxygen evolving complex of photosystem II: Jahn–Teller distortion and its suppression by Ca doping in cubane structures, Int. J. Quantum Chem. 113 (2013) 453–473.
[14] H. Dau, I. Zaharieva, M. Haumann, Recent developments in research on water oxidation by photosystem II, Curr. Opin. Chem. Biol. 16 (2012) 3–10.
[15] J. Yano, J. Kern, K.D. Irrgang, M.J. Latimer, U. Bergmann, P. Glatzel, Y. Pushkar, J. Biesiadka, B. Loll, K. Sauer, J. Messinger, A. Zouni, V.K. Yachandra, X-ray damage to the Mn4Ca complex in single crystals of photosystem II: a case study for metalloprotein crystallography, Proc. Natl. Acad. Sci. U. S. A. 102 (2005) 12047–12052.
[16] M. Grabolle, M. Haumann, C. Muller, P. Liebisch, H. Dau, Rapid loss of structural motifs in the manganese complex of oxygenic photosynthesis by X-ray irradiation at 10–300 K, J. Biol. Chem. 281 (2006) 4580–4588.
[17] D.M. Robinson, Y.B. Go, M. Mui, G. Gardner, Z. Zhang, D. Mastrogiovanni, E. Garfunkel, J. Li, M. Greenblatt, G.C. Dismukes, Photochemical water oxidation by crystalline polymorphs of manganese oxides: structural requirements for catalysis, J. Am. Chem. Soc. 135 (2013) 3494–3501.
[18] K. Kawakami, Y. Umena, N. Kamiya, J.-R. Shen, Structure of the catalytic, inorganic core of oxygen-evolving photosystem II at 1.9 Å resolution, J. Photochem. Photobiol. B 104 (2011) 9–18.
[19] M.D. Godbole, O. Roubeau, A.M. Mills, H. Kooijman, A.L. Spek, E. Bouwman, High-nuclearity manganese and iron complexes with the anionic ligand methyl salicylimidate, Inorg. Chem. 45 (2006) 6713–6722.
[20] D.M. Robinson, Y.B. Go, M. Greenblatt, G.C. Dismukes, Water oxidation by lambda-MnO_2: catalysis by the cubical Mn_4O_4 subcluster obtained by delithiation of spinel $LiMn_2O_4$, J. Am. Chem. Soc. 132 (2010) 11467–11469.
[21] J.P. McEvoy, G.W. Brudvig, Water-splitting chemistry of photosystem II, Chem. Rev. 106 (2006) 4455–4483.
[22] M.J. Latimer, V.J. DeRose, V.K. Yachandra, K. Sauer, M.P. Klein, Structural effects of calcium depletion on the manganese cluster of Photosystem II: determination by X-ray absorption spectroscopy, J. Phys. Chem. B 102 (1998) 8257–8265.
[23] T. Lohmiller, N. Cox, J.H. Su, J. Messinger, W. Lubitz, The basic properties of the electronic structure of the oxygen-evolving complex of photosystem II are not perturbed by Ca^{2+} removal, J. Biol. Chem. 287 (2012) 24721–24733.
[24] A. Boussac, A.W. Rutherford, Nature of the inhibition of the oxygen-evolving enzyme of photosystem II induced by sodium chloride washing and reversed by the addition of Ca^{2+} or Sr^{2+}, Biochemistry 27 (1988) 3476–3483.
[25] J.S. Vrettos, D.A. Stone, G.W. Brudvig, Quantifying the ion selectivity of the Ca^{2+} site in photosystem II: evidence for direct involvement of Ca^{2+} in O_2 formation, Biochemistry 40 (2001) 7937–7945.
[26] V.K. Yachandra, J. Yano, Calcium in the oxygen-evolving complex: structural and mechanistic role determined by X-ray spectroscopy, J. Photochem. Photobiol. B 104 (2011) 51–59.
[27] F.H. Koua, Y. Umena, K. Kawakami, J.R. Shen, Structure of Sr-substituted photosystem II at 2.1 Å resolution and its implications in the mechanism of water oxidation, Proc. Natl. Acad. Sci. U. S. A. 110 (2013) 3889–3894.
[28] F. Rappaport, N. Ishida, M. Sugiura, A. Boussac, Ca_{2+} determines the entropy changes associated with the formation of transition states during water oxidation by Photosystem II, Energy Environ. Sci. 4 (2011) 2520–2524.
[29] Y. Pushkar, J. Yano, K. Sauer, A. Boussac, V.K. Yachandra, Structural changes in the Mn_4Ca cluster and the mechanism of photosynthetic water splitting, Proc. Natl. Acad. Sci. U. S. A. 105 (2008) 1879–1884.
[30] A. Boussac, F. Rappaport, P. Carrier, J.M. Verbavatz, R. Gobin, D. Kirilovsky, A.W. Rutherford, M. Sugiura, Biosynthetic Ca^{2+}/Sr^{2+} exchange in the photosystem II oxygen-evolving enzyme of *Thermosynechococcus elongatus*, J. Biol. Chem. 279 (2004) 22809–22819.
[31] T.-A. Ono, Y. Inoue, Discrete extraction of the Ca atom functional for O_2 evolution in higher plant photosystem II by a simple low pH treatment, FEBS Lett. 227 (1988) 147–152.
[32] M. Sivaraja, J. Tso, G.C. Dismukes, A calcium-specific site influences the structure and activity of the manganese cluster responsible for photosynthetic water oxidation, Biochemistry 28 (1989) 9459–9464.
[33] A. Boussac, J.-L. Zimmermann, A.W. Rutherford, EPR signals from modified charge accumulation states of the oxygen-evolving enzyme in Ca^{2+}-deficient photosystem II, Biochemistry 28 (1989) 8984–8989.
[34] B.R. Brooks, R.E. Bruccoleri, B.D. Olafson, D.J. States, S. Swaminathan, M. Karplus, CHARMM: a program for macromolecular energy minimization and dynamics calculations, J. Comput. Chem. 4 (1983) 187–217.
[35] A.D. MacKerell Jr., D. Bashford, R.L. Bellott, R.L. Dunbrack Jr., J.D. Evanseck, M.J. Field, S. Fischer, J. Gao, H. Guo, S. Ha, D. Joseph-McCarthy, L. Kuchnir, K. Kuczera, F.T.K. Lau, C. Mattos, S. Michnick, T. Ngo, D.T. Nguyen, B. Prodhom, W.E. Reiher III, B. Roux, M. Schlenkrich, J.C. Smith, R. Stote, J. Straub, M. Watanabe, J. Wiorkiewicz-Kuczera, D. Yin, M. Karplus, All-atom empirical potential for molecular modeling and dynamics studies of proteins, J. Phys. Chem. B 102 (1998) 3586–3616.
[36] K. Saito, T. Ishida, M. Sugiura, K. Kawakami, Y. Umena, N. Kamiya, J.-R. Shen, H. Ishikita, Distribution of the cationic state over the chlorophyll pair of photosystem II reaction center, J. Am. Chem. Soc. 133 (2011) 14379–14388.
[37] QSite, version 5.8, Schrödinger, LLC, New York, NY, 2012.
[38] K. Saito, J.-R. Shen, T. Ishida, H. Ishikita, Short hydrogen-bond between redox-active tyrosine Y_Z and D1-His190 in the photosystem II crystal structure, Biochemistry 50 (2011) 9836–9844.
[39] S.L. Dexheimer, M.P. Klein, Detection of a paramagnetic intermediate in the S1 state of the photosynthetic oxygen-evolving complex, J. Am. Chem. Soc. 114 (1992) 2821–2826.
[40] T. Yamauchi, H. Mino, T. Matsukawa, A. Kawamori, T. Ono, Parallel polarization electron paramagnetic resonance studies of the S1-state manganese cluster in the photosynthetic oxygen-evolving system, Biochemistry 36 (1997) 7520–7526.
[41] R.D. Britt, J.M. Peloquin, K.A. Campbell, Pulsed and parallel-polarization EPR characterization of the photosystem II oxygen-evolving complex, Annu. Rev. Biophys. Biomol. Struct. 29 (2000) 463–495.
[42] W. Ames, D.A. Pantazis, V. Krewald, N. Cox, J. Messinger, W. Lubitz, F. Neese, Theoretical evaluation of structural models of the S_2 state in the oxygen evolving complex of Photosystem II: protonation states and magnetic interactions, J. Am. Chem. Soc. 133 (2011) 19743–19757.
[43] H. Isobe, M. Shoji, S. Yamanaka, Y. Umena, K. Kawakami, N. Kamiya, J.R. Shen, K. Yamaguchi, Theoretical illumination of water-inserted structures of the $CaMn_4O_5$ cluster in the S2 and S3 states of oxygen-evolving complex of photosystem II: full geometry optimizations by B3LYP hybrid density functional, Dalton Trans. 41 (2012) 13727–13740.
[44] P.E. Siegbahn, Structures and energetics for O_2 formation in photosystem II, Acc. Chem. Res. 42 (2009) 1871–1880.
[45] S. Luber, I. Rivalta, Y. Umena, K. Kawakami, J.-R. Shen, N. Kamiya, G.W. Brudvig, V.S. Batista, S_1-state model of the O_2-evolving complex of photosystem II, Biochemistry 50 (2011) 6308–6311.
[46] C.P. Aznar, R.D. Britt, Simulations of the ^{1}H electron spin echo-electron nuclear double resonance and ^{2}H electron spin echo envelope modulation spectra of exchangeable hydrogen nuclei coupled to the S_2-state photosystem II manganese cluster, Philos. Trans. R. Soc. Lond. B Biol. Sci. 357 (2002) 1359–1365.
[47] R.D. Britt, K.A. Campbell, J.M. Peloquin, M.L. Gilchrist, C.P. Aznar, M.M. Dicus, J. Robblee, J. Messinger, Recent pulsed EPR studies of the photosystem II oxygen-evolving complex: implications as to water oxidation mechanisms, Biochim. Biophys. Acta 1655 (2004) 158–171.
[48] H. Dau, M. Haumann, The manganese complex of photosystem II in its reaction cycle? Basic framework and possible realization at the atomic level, Coord. Chem. Rev. 252 (2008) 273–295.
[49] J.S. Kanady, E.Y. Tsui, M.W. Day, T. Agapie, A synthetic model of the Mn_3Ca subsite of the oxygen-evolving complex in photosystem II, Science 333 (2011) 733–736.
[50] S. Mukherjee, J.A. Stull, J. Yano, T.C. Stamatatos, K. Pringouri, T.A. Stich, K.A. Abboud, R.D. Britt, V.K. Yachandra, G. Christou, Synthetic model of the asymmetric [Mn3CaO4] cubane core of the oxygen-evolving complex of photosystem II, Proc. Natl. Acad. Sci. U. S. A. 109 (2012) 2257–2262.
[51] G.C. Dismukes, Y. Siderer, Intermediates of a polynuclear manganese center involved in photosynthetic oxidation of water, Proc. Natl. Acad. Sci. U. S. A. 78 (1981) 274–278.
[52] A. Boussac, J.J. Girerd, A.W. Rutherford, Conversion of the spin state of the manganese complex in photosystem II induced by near-infrared light, Biochemistry 35 (1996) 6984–6989.
[53] A. Boussac, S. Un, O. Horner, A.W. Rutherford, High-spin states ($S \geq 5/2$) of the photosystem II manganese complex, Biochemistry 37 (1998) 4001–4007.
[54] A. Boussac, A.W. Rutherford, Comparative study of the $g = 4.1$ EPR signals in the S_2 state of photosystem II, Biochim. Biophys. Acta 1457 (2000) 145–156.
[55] K. Saito, A.W. Rutherford, H. Ishikita, Mechanism of tyrosine D oxidation in Photosystem II, Proc. Natl. Acad. Sci. U. S. A. 110 (2013) 7690–7695.
[56] A. Boussac, P. Setif, A.W. Rutherford, Inhibition of tyrosine Z photooxidation after formation of the S3-state in Ca^{2+}-depleted and Cl^{-}-depleted photosystem II, Biochemistry 31 (1992) 1224–1234.
[57] P. van Vliet, A.W. Rutherford, Properties of the chloride-depleted oxygen-evolving complex of photosystem II studied by electron paramagnetic resonance, Biochemistry 35 (1996) 1829–1839.
[58] H. Wincencjusz, H.J. van Gorkom, C.F. Yocum, The photosynthetic oxygen evolving complex requires chloride for its redox state S2 → S3 and S3 → S0 transitions but not for S0 → S1 or S1 → S2 transitions, Biochemistry 36 (1997) 3663–3670.